22. Schnitzer, I., Yablonovitch, E., Caneau, C., Gmitter, T. J. & Scherer, A. 30% external quantum efficiency from surface textured, thin-film light-emitting diodes. *Appl. Phys. Lett.* **63,** 2174–2176 (1993).
23. Fricke, J., Yang, B., Brandt, O. & Ploog, K. Patterning of cubic and hexagonal GaN by $Cl_2/N_2$-based reactive ion etching. *Appl. Phys. Lett.* **74,** 3471–3473 (1999).

**Acknowledgements**

We thank O. Mayrock and H.-J. Wünsche for help in the calculation of single-particle wavefunctions and exciton binding energies. This work was supported in part by the Volkswagen-Stiftung.

Correspondence and requests for materials should be addressed to P.W. (e-mail: walter@pdi-berlin.de).

# Liquid crystal phase transitions in suspensions of polydisperse plate-like particles

**Felix M. van der Kooij, Katerina Kassapidou & Henk N. W. Lekkerkerker**

*Van't Hoff Laboratory for Physical and Colloid Chemistry, Debye Institute, Utrecht University, Padualaan 8, 3584 CH Utrecht, The Netherlands*

**Colloidal suspensions that form periodic self-assembling structures on sub-micrometre scales are of potential technological interest; for example, three-dimensional arrangements of spheres in colloidal crystals[1] might serve as photonic materials[2], intended to manipulate light. Colloidal particles with non-spherical shapes (such as rods and plates) are of particular interest because of their ability to form liquid crystals. Nematic liquid crystals possess orientational order; smectic and columnar liquid crystals additionally exhibit positional order (in one or two dimensions respectively). However, such positional ordering[3,4] may be inhibited in polydisperse colloidal suspensions. Here we describe a suspension of plate-like colloids that shows isotropic, nematic and columnar phases on increasing the particle concentration. We find that the columnar two-dimensional crystal persists for a polydispersity of up to 25%, with a cross-over to smectic-like ordering at very high particle concentrations. Our results imply that liquid crystalline order in synthetic mesoscopic materials may be easier to achieve than previously thought.**

Suspensions of (almost) monodisperse colloidal particles are used as mesoscopic models of the phase behaviour of atomic and molecular systems. In this respect, the fluid–crystal transition in suspensions of spheres[1] and the liquid crystal phase transitions in suspensions of non-spherical particles[5,6] have attracted considerable attention. However, colloidal particles are hardly ever truly monodisperse but often exhibit a size distribution of finite width. The consequences of this inherent polydispersity are of substantial fundamental and industrial interest. In particular, the inhibitive role of polydispersity in the crystallization process of hard spheres is a contentious issue that deals with the value[3,7–9] and even the very existence[10,11] of a so-called terminal polydispersity $\sigma_t$, above which no crystallization can occur.

Moreover, one may wonder how polydispersity affects positional ordering if such ordering exists in just one or two dimensions, that is, in the case of smectic or columnar liquid crystals (sketched in Fig. 1). Driven by a gain in excluded volume entropy, these liquid crystal phases may be formed in concentrated suspensions of hard-body rod or plate-like particles[12,13]. For dense systems of rods, computer simulation predicts a stable smectic phase up to a polydispersity in rod length of 18%, while for higher polydispersities the smectic phase is pre-empted by a columnar phase[4]. Accordingly, in experiments, almost monodisperse rod-like virus particles show a smectic phase[6] while polydisperse solutions of DNA-rods show a columnar phase instead[14].

The phase behaviour of hard plate-like particles, on the other hand, has received considerably less attention, largely because suitable experimental model systems have been developed only recently[15,16]. One of these model systems, comprising fairly monodisperse platelets of low aspect ratio, exhibits an isotropic and columnar phase[17]; but, computer simulation for monodisperse platelets of sufficiently large aspect ratio predicts an isotropic (I),

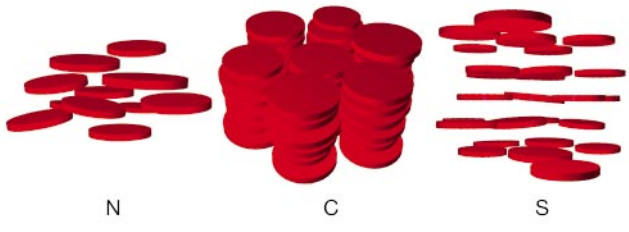


**Figure 1** Structure of the three main classes of liquid crystals. The nematic phase (N), the columnar phase (C), and the smectic phase (S) are schematically depicted here for the case of plate-like particles. While each of these phases exhibits long-range orientational order, they differ by the positional correlations between the particles. In the nematic phase long-range positional order is absent. The columnar phase has a two-dimensional lattice of columns, which are constituted of liquid-like stacks of particles. The smectic phase is characterized by a one-dimensional periodic array of layers of particles.

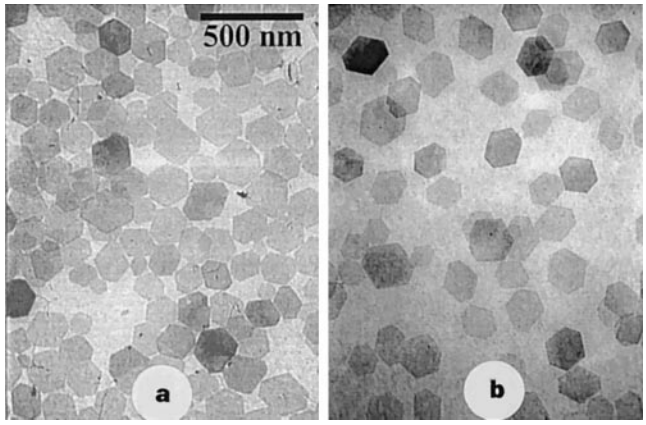


**Figure 2** Transmission electron microscopy images. **a**, The parent suspension ($\sigma_D = 25\%$); and **b**, the fractionated suspension ($\sigma_D = 17\%$). The platelets are gibbsite (that is, $Al(OH_3)$) colloids whose surface is grafted with a modified polyisobutylene ($M_w \approx 1{,}000$ g per mole). Owing to this steric stabilization layer, the particles interact through an approximately hard-core (that is, short-range repulsive) interaction potential when dispersed in apolar solvents (in this case, toluene)[15,23]. The reduction of the particles' polydispersity in diameter to 17% is achieved by fractionation of part of the parent system, using a scheme which resembles the method of depletion-enhanced crystallization fractionation of emulsion droplets as described[24]. The suspension is submitted to I–N phase separation, using $\pm 2$ g $l^{-1}$ added non-adsorbing polymer to enhance fractionation, yielding roughly 80% nematic phase in coexistence with 20% isotropic phase. The isotropic upper phase is subsequently removed. By dilution of the remaining nematic phase (using polymer solution) back to the I–N region and repeating this scheme twice, the suspension thus obtained has a lower polydispersity than the original system. The non-adsorbing polymer is subsequently removed by redispersioning in polymer-free solvent after sedimentation. The number-average diameter $\langle D \rangle$ of the grafted platelets (Table 2) is based on the diameter of the core, determined from transmission electron microscopy (TEM) micrographs, plus twice the estimated thickness (4 nm) of the grafted polymer layer[25]. We define the diameter of the hexagons by the diameter of a circle of equal area, with a relative standard deviation $\sigma_D = (\langle D^2 \rangle - \langle D \rangle^2)^{1/2} / \langle D \rangle$. The number-average thickness $\langle L \rangle$ of the plates (including the grafted polymer layer) is roughly 14 nm, with a standard deviation which is experimentally not readily accessible but probably lower than that in diameter[26].

a nematic (N), and a columnar (C) phase upon increasing the concentration of platelets[13,18–21]. The isotropic to nematic (I–N) phase transition, which does not involve positional order (see Fig. 1), has recently been observed in experiments on suspensions of gibbsite platelets[15]. In the present study we explore the liquid crystal phase behaviour of these fairly polydisperse suspensions at higher densities, where simulations predict a N–C transition in the monodisperse case. We consider two systems which differ by the degree of polydispersity in diameter of the constituent platelets (17 and 25%, respectively, see Fig. 2). A dimension-based speculation on the terminal polydispersity for columnar ordering of plates, which can be considered as two-dimensional crystallization, would yield a value in the range 5–20%, falling between the values for three-dimensional crystallization of spheres and for one-dimensional smectic ordering of rods.

This raises the following questions. Do suspensions of plates, particularly in the studied range of polydispersity, show a nematic–columnar phase transition as predicted for monodisperse plates? Or do they, in order to circumvent the effect of polydispersity in diameter, form a smectic phase instead? What is the role and extent of particle size partitioning between coexisting phases?

The phase behaviour of the platelet suspensions as a function of the plate volume fraction is presented in Fig. 3. Isotropic–nematic phase coexistence is observed just below $\phi = 0.2$, yielding an isotropic upper phase and a birefringent nematic bottom phase. Macroscopic phase separation is complete within 12 hours. The width of the biphasic region $\Delta\phi_{IN}$ depends strongly on the polydispersity in diameter $\sigma_D$, $\Delta\phi_{IN}$ being twice as broad for the suspension with $\sigma_D = 25\%$ compared to that with $\sigma_D = 17\%$ (Fig. 4). This observation is consistent with the relation $\Delta\phi_{IN} \propto \sigma^2$ as found in computer simulations for polydisperse disks[20].

Upon increasing the plate volume fraction to roughly twice the I–N coexistence density, $\phi \approx 0.4$, both the suspension of 17 and 25% polydispersity enter a biphasic region where a nematic upper phase coexists with a more concentrated birefringent bottom phase. A columnar signature of the lower phase is suggested by unequivocal Bragg reflections when illuminated by white light (Fig. 3). The fact that these reflections appear for wavelengths of visible light demonstrates that the crystalline order pertains to a periodicity on a length scale of the plate diameter (characteristic of columnar ordering) rather than the much smaller plate thickness (as in smectic ordering). By applying Bragg's law to the angle of reflection measured for different wavelengths of light, we identify the characteristic spacing (of the (100) reflection, see small-angle X-ray scattering (SAXS) results) as 219 ± 5 nm and 214 ± 5 nm for the parent and fractionated suspensions, respectively. This corresponds to a typical distance between the centres of the columns of 253 ± 6 and 247 ± 6 nm. A comparison of the experimentally observed I–N and N–C transition densities to computer simulations for monodisperse hard disks[13], as depicted in Fig. 4, shows that the transitions in the experiment are shifted to slightly lower densities. The difference in shape of the platelets studied (hexagonal in the experiment versus circular in the simulation) we expect to be a major contribution to this shift, as shown recently for the I–N transition[21]. Macroscopic phase separation in the N–C biphasic gap is complete within 2 weeks.

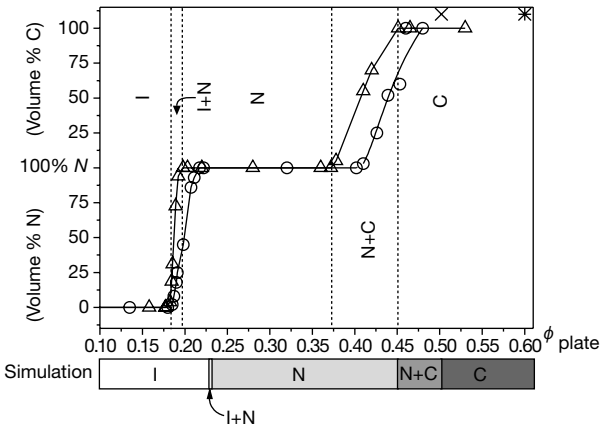


**Figure 4** Phase diagram of the suspensions. The relative volume of the nematic and columnar phase are depicted after phase separation as a function of the platelet volume fraction $\phi$. Results apply to $\sigma_D = 17\%$ (triangles) and $\sigma_D = 25\%$ (circles), respectively. The points marked by a cross and a star belong to the latter system but at densities beyond columnar stability, corresponding to curves **c** and **d**, respectively, in Fig. 5. The dotted lines indicate the boundaries of the coexistence regions of the suspension with $\sigma_D = 17\%$. Results from computer simulation[13] for monodisperse hard disks, extrapolated to the current aspect ratio $\langle D\rangle/\langle L\rangle$ of roughly 13, are included for comparison.

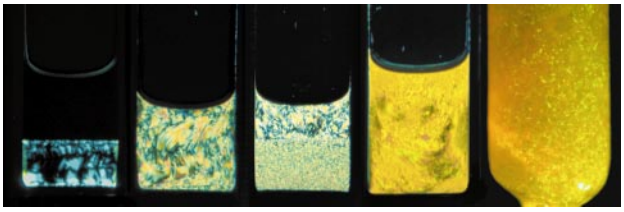

**Figure 3** Tubes containing suspensions at varying concentrations. They are photographed between crossed polarizers to distinguish between isotropic (dark) and the birefringent nematic and columnar liquid crystalline phases. The suspensions depicted here comprise platelets with 17% polydispersity in diameter. From left to right, the concentration ranges from $\phi = 0.19$ (I + N), 0.28 (N), 0.41 (N + C), to 0.47 (C). The tube to the far right depicts the monophasic columnar sample at $\phi = 0.45$ as observed without polarizers but illuminated by white light. The colours of its Bragg reflections (visible as small bright spots) vary from yellow to green, as the angle between the incident light and viewing direction is in the range 50–70°. The particle volume fraction $\phi$ (which includes the solvent immobilized in the grafted polymer layer) is calculated as the mass concentration (determined by drying a known amount of dispersion to constant weight at 75 °C) divided by the effective mass density of the grafted particles. Following ref. 27, the latter is derived from the TEM particle dimensions, the estimated thickness of the stabilizing layer[25], the polymer mass fraction from elemental analysis and the mass density of gibbsite[28]. This yields a mass density of about 1.3 g cm$^{-3}$, with an estimated error of 10% that is due to the uncertainty in polymer layer thickness.

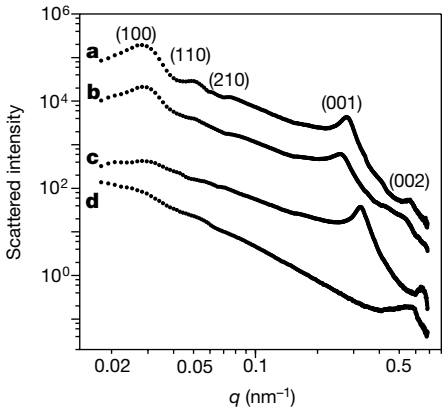


**Figure 5** Small angle X-ray scattering patterns for samples varying in polydispersity and volume fraction. **a**, $\sigma_D = 17\%$ at $\phi = 0.45$, **b**–**d**, $\sigma_D = 25\%$ at $\phi = 0.45$, 0.5 and 0.6 respectively. Curves **a** and **b** correspond to a columnar phase, curve **c** to smectic-like ordering at densities above columnar stability, and curve **d** depicts the glassy state encountered upon increasing the density even further. Curves shown are radially averaged scattered intensities, in arbitrary units, as a function of the scattering vector $q = 4\pi/\lambda\sin(\theta/2)$, with $\theta$ the scattering angle. Experiments are performed at the DUBBLE beam line at the European Synchroton Radiation Facility, France.

**Table 1 $q$ values of the scattering peaks in the SAXS pattern**

| Sample | $\sigma_D$ (%) | $\phi$ | $q$ ($10^{-2}$ nm$^{-1}$) (100) | (110) | (210) | (001) | (002) |
|---|---|---|---|---|---|---|---|
| *a* | 17 | 0.45 | 2.82 | 4.88 | 7.40 | 27.8 | 55.5 |
| *b* | 25 | 0.45 | 2.89 | 5.00 | 7.44 | 25.6 | |
| *c* | 25 | 0.5 | (2.88) | | | 32.3 | 64.4 |

SAXS experiments provide further proof for the columnar signature of the dense liquid crystal phase. Curves **a** and **b** in Fig. 5 correspond to the columnar phase in the case of 17 and 25% polydispersity, respectively. These curves show almost identical features. In the small $q$ regime, where the spacing $d = 2\pi/q$ is of the order of the diameter of the plates, we can distinguish one major peak and two additional peaks. The $q$ values of these three peaks (Table 1), whose $q$ ratio is like $1 : \sqrt{3} : \sqrt{7}$, reveals that ordering in the plane of the plate diameters is hexagonal, with the peaks corresponding to the (100), (110) and (210) reflections. The (200) reflection seems to be relatively weak compared to its neighbouring (110) and (210) peaks, such that it is not (clearly) resolved in the scattering profile. From the $q$ values of the (100), (110) and (210) peaks we obtain the typical distance between the centres of the columns to be $251 \pm 4$ and $258 \pm 1$ nm in the suspension with $\sigma_D = 25\%$ and 17%, respectively, in good agreement with the values found with light scattering. This distance is hence almost equal to $(1 + \sigma_D) \times D$ for both suspensions. The two peaks at much larger $q$ correspond to 1 and 0.5 times a spacing of roughly the plate thickness, such that we identify them as (001) and (002) reflections. These peaks may therefore relate to (liquid-like) order between the plates along the $z$-axis of a column of plates. Although the observed scattering patterns are consistent with a columnar structure, they could also stem from a structure in which particles are hexagonally ordered in layers without lateral correlations between adjacent layers. These structures can be distinguished by orienting a single crystal in the X-ray beam with the beam parallel to the plate normals[17,22]. If the structure is columnar, tilting the sample with respect to the beam will not result in a change in $q$ values of the scattering peaks, similar to the behaviour of a three-dimensional crystal of spheres. Tilting a sample in a 0.2-mm flat capillary (approximating a single crystal) indeed does not lead to a significant (>1%) shift in the $q$ positions of the scattering peaks. Apart from the unlikely (though not excluded) possibility of a three-dimensional crystal structure, the tilting experiment thus confirms that the dense liquid crystal phase is a columnar phase.

A remaining question concerns the origin of the observed columnar stability in these systems where polydispersity must be an important factor. In analogy with computer simulations' predictions for crystallization of polydisperse hard spheres, stabilization of the ordered phase may emanate from fractionation, lowering the polydispersity in the ordered phase at the expense of the polydispersity in a coexisting disordered phase. In the present study we can determine the extent of fractionation experimentally, by examination (using transmission electron microscopy, TEM) of small samples of a coexisting nematic and columnar phase. Fractionation indeed gives rise to a reduction of the polydispersity in the columnar phase, as we find $\sigma_D = 18$ and 14% in the columnar phase of the two systems studied (Table 2). This indicates that at least the pre-fractionated system ($\sigma_D = 17\%$) should be able to enter a monophasic columnar state beyond the N–C coexistence region. In fact, the fully columnar state is observed for both suspensions. This demonstrates that even in the case of $\sigma_D = 25\%$ fractionation is not an absolute condition for columnar ordering, and that this polydispersity in diameter is therefore still below the terminal value. One may wonder, however, whether the columnar structure will persist upon increasing the volume fraction of a fully columnar sample, that is, if the spacing between the columns decreases such that the disruptive effect of polydispersity in diameter becomes more pronounced. For $\phi = 0.50$ (curve **c** in Fig. 5), the columnar (100), (110) and (210) peaks in a sample of $\sigma_D = 25\%$ become markedly suppressed, whereas, at the same time, the (001) and (002) peaks become more distinct. Bragg reflections for visible light (which pertain to the (100) reflection) almost completely disappear. We speculate that the suppression of the columnar peaks and the simultaneous structuring with a periodicity of the order of the plate thickness is indicative of a cross-over to smectic-like ordering. Unlike the columnar phase, a smectic phase is not sensitive to polydispersity in diameter, as ordering within the smectic layers is liquid-like. Instead, the smectic requires a low polydispersity in thickness. The relative stability of the nematic, columnar and smectic phases is therefore determined not only by the volume fraction of the suspension and the polydispersity in diameter, but also by polydispersity in thickness. Our observation that a system with $\sigma_D$ as high as 25% forms a columnar phase, and its cross-over to a smectic-like structure at higher $\phi$, are therefore probably connected with the fact that the platelets have a polydispersity in thickness too. Indeed, in the case of $\sigma_D = 17\%$, the columnar phase is still stable at $\phi = 0.53$ as demonstrated by strong Bragg reflections for visible light.

The stability of a columnar phase in these polydisperse suspensions of plates seems remarkable in the light of predictions for the terminal polydispersity for the crystal phase of hard spheres and smectic phase for hard rods, although in the latter only polydispersity in length is taken into account. Further insight into the stability of the nematic, columnar and smectic phase in systems of polydisperse plates therefore requires study by computer simulation, addressing the role of polydispersity in both diameter and thickness. □

**Table 2 Fractionation in the N–C coexistence region**

| System | Overall | | N-phase | | C-phase | |
|---|---|---|---|---|---|---|
| | $\langle D \rangle$ (nm) | $\sigma_D$ (%) | $\langle D \rangle$ (nm) | $\sigma_D$ (%) | $\langle D \rangle$ (nm) | $\sigma_D$ (%) |
| I | 198 | 25 | 196 | 26 | 200 | 18 |
| II | 212 | 17 | 209 | 18 | 220 | 14 |

The diameter distributions of the parent (I) and the pre-fractionated system (II), before and after N–C phase separation. Values are determined from TEM micrographs by measuring about 200 particles in each case.

Received 26 April; accepted 4 July 2000.


1. Pusey, P. N. & van Megen, W. Phase behaviour of concentrated suspensions of nearly hard spheres. *Nature* **320,** 340–342 (1986).
2. Blanco, A. *et al.* Large-scale synthesis of a silicon photonic crystal with a complete three-dimensional bandgap near 1.5 micrometers. *Nature* **405,** 437–440 (2000).
3. Pusey, P. N. in *Les Houches, Session LI, Liquids, Freezing & Glass Transitions* Ch. 10 (North-Holland, Amsterdam, 1991).
4. Bates, M. & Frenkel, D. Influence of polydispersity on the phase behavior of colloidal liquid crystals: A Monte Carlo study. *J. Chem. Phys.* **109,** 6193–6199 (1998).
5. Bernal, J. D. & Fankuchen, I. X-ray and crystallographic studies of plant virus preparations. *J. Gen. Physiol.* **25,** 111–146 (1941).
6. Dogic, Z. & Fraden, S. Smectic phase in a colloidal suspension of semiflexible virus particles. *Phys. Rev. Lett.* **78,** 2417–2420 (1997).
7. Pusey, P. N. The effect of polydispersity on the crystallization of hard spherical colloids. *J. Phys. (Paris)* **48,** 709–712 (1987).
8. Barrat, J. L. & Hansen, J. P. On the stability of polydisperse colloidal crystals. *J. Phys. (Paris)* **46,** 1547–1553 (1986).
9. McRae, R. & Haymet, A. D. J. Freezing of polydisperse hard spheres. *J. Chem. Phys.* **88,** 1114–1125 (1988).
10. Bolhuis, P. G. & Kofke, D. A. Monte Carlo study of freezing of polydisperse hard spheres. *Phys. Rev. E* **54,** 634–643 (1996).
11. Kofke, D. A. & Bolhuis, P. G. Freezing of polydisperse hard spheres. *Phys. Rev. E* **59,** 618–622 (1999).
12. Frenkel, D., Lekkerkerker, H. N. W. & Stroobants, A. Thermodynamic stability of a smectic phase in a system of hard rods. *Nature* **332,** 822–823 (1988).
13. Veerman, J. A. C. & Frenkel, D. Phase behavior of disklike hard-core mesogens. *Phys. Rev. A* **45,** 5632–5648 (1992).
14. Livolant, F., Levelut, A. M., Doucet, J. & Benoit, J. P. The concentrated DNA liquid crystalline phase is columnar hexatic. *Nature* **339,** 724–728 (1989).
15. van der Kooij, F. M. & Lekkerkerker, H. N. W. Formation of nematic liquid crystals in suspensions of hard colloidal platelets. *J. Phys. Chem. B* **102,** 7829–7832 (1998).
16. Brown, A. B. D., Clarke, S. M. & Rennie, A. R. Ordered phase of platelike particles in concentrated dispersions. *Langmuir* **14,** 3129–3132 (1998).

17. Brown, A. B. D., Ferrero, C., Narayanan, T. & Rennie, A. R. Phase separation and structure in a concentrated colloidal dispersion of uniform plates. *Eur. Phys. J. B* **11,** 481–489 (1999).
18. Onsager, L. The effect of shape on the interaction of colloidal particles. *Ann. NY Acad. Sci.* **51,** 627–659 (1949).
19. Frenkel, D. & Eppenga, R. Monte Carlo study of the isotropic-nematic transition in a fluid of thin hard disks. *Phys. Rev. Lett.* **52,** 1089–1092 (1982).
20. Bates, M. & Frenkel, D. Nematic-isotropic transition in polydisperse systems of infinitely thin hard platelets. *J. Chem. Phys.* **110,** 6553–6559 (1999).
21. Bates, M. Influence of particle shape on the nematic-isotropic transition of colloidal platelet systems. *J. Chem. Phys.* **111,** 1732–1736 (1999).
22. Guinier, A. *X-ray Diffraction in Crystals, Imperfect Crystals, & Amorphous Bodies* 169–172 (Dover, New York, 1994).
23. van der Kooij, F. M., Philipse, A. P. & Dhont, J. K. G. Sedimentation and diffusion in suspensions of sterically stabilized colloidal platelets. *Langmuir* **16,** 5317–5323 (2000).
24. Bibette, JU. Depletion interactions and fractionated crystallisation for polydisperse emulsion purification. *J. Colloid Interface Sci.* **147,** 474–478 (1991).
25. Smits, C., Briels, W. J., Dhont, J. K. G. & Lekkerkerker, H. N. W. Influence of the stabilizing coating on the rate of crystallization of colloidal suspensions. *Prog. Colloid Polym. Sci.* **79,** 287–292 (1989).
26. van der Kooij, F. M. & Lekkerkerker, H. N. W. The liquid crystalline phase behaviour of a colloidal rod-plate mixture. *Phys. Rev. Lett.* **84,** 781–784 (2000).
27. van Bruggen, M. P. B., Dhont, J. K. G. & Lekkerkerker, H. N. W. Morphology and kinetics of the isotropic-nematic phase transition in dispersions of hard rods. *Macromolecules* **32,** 2256–2264 (1999).
28. Gitzen, W. H. *Alumina as a Ceramic Material* 31 (The American Ceramic Society, Columbus, 1970).

**Acknowledgements**

We thank A. R. Rennie for discussions concerning the columnar phase, I. Dolbnya and W. Bras for technical support at DUBBLE, and D. Frenkel for a critical reading of the manuscript. This work was supported by the Foundation for Fundamental Research on Matter (FOM) and the Netherlands Organization for the Advancement of Research (NWO).

Correspondence should be addressed to H.L. (e-mail: H.N.W.Lekkerkerker@chem.uu.nl).

# Multiscale modelling of plastic flow localization in irradiated materials

**Tomas Diaz de la Rubia*, Hussein M. Zbib†, Tariq A. Khraishi†, Brian D. Wirth*, Max Victoria‡ & Maria Jose Caturla***

* *Lawrence Livermore National Laboratory, 7000 East Avenue, L-353, Livermore, California 94550, USA*
† *Washington State University, School of Mechanical & Materials Engineering, Pullman, Washington 99164, USA*
‡ *EPFL-CRPP-Fusion Technology Materials, 5232 Villigen PSI, Switzerland*

**The irradiation of metals by energetic particles causes significant degradation of the mechanical properties[1,2], most notably an increased yield stress and decreased ductility, often accompanied by plastic flow localization. Such effects limit the lifetime of pressure vessels in nuclear power plants[3], and constrain the choice of materials for fusion-based alternative energy sources[4]. Although these phenomena have been known for many years[1], the underlying fundamental mechanisms and their relation to the irradiation field have not been clearly demonstrated. Here we use three-dimensional multiscale simulations of irradiated metals to reveal the mechanisms underlying plastic flow localization in defect-free channels. We observe dislocation pinning by irradiation-induced clusters of defects, subsequent unpinning as defects are absorbed by the dislocations, and cross-slip of the latter as the stress is increased. The width of the plastic flow channels is limited by the interaction among opposing dislocation dipole segments and the remaining defect clusters.**

The microstructure of irradiated materials evolves over a wide range of length and time scales, making radiation damage an inherently multiscale phenomenon. At the shortest scales (nanometres and picoseconds), recoil-induced cascades of energetic atomic displacements give rise to a highly non-equilibrium concentration of point defects and point defect clusters[5]. Over macroscopic length and time scales these defects can migrate and alter the chemistry and microstructure, often inducing significant degradation of mechanical and other properties[1,2]. In metals, the main features of neutron or ion beam irradiation-induced mechanical behaviour can be summarized as[2]: (1) a sharp increase in yield stress with irradiation dose; (2) the appearance of a yield point followed by a yield drop in f.c.c. metals; and (3) an instability that results in plastic flow localization within 'dislocation channels' and leads to loss of ductility and premature failure. An example of flow localization is shown in Fig. 1 (ref. 6). The transmission electron microscopy image shows a channel where all visible irradiation-induced point defect clusters are absent and where uniform large shear (about 100%) has taken place. The channels are 100 to 200 nm wide. Plastic flow localization is responsible for the observed loss of ductility.

Early theories of irradiation hardening focused on various source and dispersed barrier mechanisms[7,8]. Recently[9,10], the analytical cascade-induced source hardening (CISH) model was proposed[9,10]. This model uses insights from molecular dynamics simulations[11–14] and accounts for some of the recent experimental observations. In the model, it is postulated that interstitial clusters produced in displacement cascades form glissile dislocation loops that migrate in one dimension by thermally activated glide, and decorate dislocations, thereby pinning them. However, while this model provides a rational explanation for the observed increase in yield stress, it does not account for plastic flow localization and the development of plastic instabilities.

Here we couple these experimental and atomistic simulation results[11–18] to a three-dimensional dislocation dynamics (DD) simulation to investigate the relation between the irradiation field and mechanical behaviour. We consider two cases, Cu and Pd, which exhibit different damage morphologies under irradiation. Experiments have shown that vacancy stacking-fault tetrahedra (SFT) are the predominant defect type in low stacking fault energy Cu[6,19], whereas in high stacking fault energy Pd, self-interstitial atom Frank sessile loops constitute the majority of observed defects[20,21]. Our DD simulation box is a cube 5 μm in size that contains an initial density of Frank–Read dislocation sources distributed at random on {111} planes. In our DD simulation[22–24], the plastic deformation of a single crystal is obtained by explicit accounting of the dislocation evolution history, that is, their motion and structure.

The motion and interaction of an ensemble of dislocations in a three-dimensional crystal is marched in time. Dislocations are discretized into straight-line segments of mixed character. The Peach–Koehler force $F$ acting on a dislocation segment inside the computational cell is calculated from the stress fields that are caused by immediate neighbouring segments, all other dislocations segments, all defect clusters and the applied stress. The result is used to advance the dislocation segment based on a linear mobility model, $v_{gi} = M_{gi}F_{gi}$, where $v_{gi}$ is the glide velocity of the dislocation segment, $M_{gi}$ is the dislocation mobility, and $F_{gi}$ is the glide component of the Peach–Koehler force minus the Peierl's friction. On the basis of the history of dislocation motion, we obtain a measure for the macroscopic plastic strain rate. To ensure continuity of dislocation lines across the boundaries, we apply reflection boundary conditions[22]. Due to the long-range character of the dislocation stress field, long-range interactions are computed explicitly[22].

In the simulation, segments that are on the verge of experiencing short-range interactions are identified. Based on a set of physical rules, such reactions may result in the formation of junctions, jogs, dipoles, and so on. The dislocations multiply by a variety of